The Plant Cell, Vol. 14, 2233–2249, September 2002, www.plantcell.org © 2002 American Society of Plant Biologists

Oscillatory Chloride Efflux at the Pollen Tube Apex Has a Role in Growth and Cell Volume Regulation and Is Targeted by Inositol 3,4,5,6-Tetra*kis*phosphate

Laura Zonia,[a,1] Sofia Cordeiro,[b,c] Jaroslav Tupý,[a] and José A. Feijó[b,c]

[a] Institute of Experimental Botany, Academy of Sciences of the Czech Republic, Na Pernikarce 15, 160 00 Prague 6, Czech Republic

[b] Instituto Gulbenkian Ciência, R. Quinta Grande 6, PT-2780-156 Oeiras, Portugal

[c] Centro de Biotecnologia Vegetal, Department Biologia Vegetal, Faculdad Ciênicas da Universitie de Lisboa, Campo Grande Ed. C2, 1749-016 Lisboa, Portugal

Oscillatory growth of pollen tubes has been correlated with oscillatory influxes of the cations Ca^{2+}, H^+, and K^+. Using an ion-specific vibrating probe, a new circuit was identified that involves oscillatory efflux of the anion Cl^- at the apex and steady influx along the tube starting at 12 μm distal to the tip. This spatial coupling of influx and efflux sites predicts that a vectorial flux of Cl^- ion traverses the apical region. The Cl^- channel blockers 4,4′-diisothiocyanatostilbene-2,2′-disulfonic acid (DIDS) and 5-nitro-2-(3-phenylpropylamino)benzoic acid completely inhibited tobacco pollen tube growth at 80 and 20 μM, respectively. Cl^- channel blockers also induced increases in apical cell volume. The apical 50 μm of untreated pollen tubes had a mean cell volume of 3905 ± 75 μm^3. DIDS at 80 μM caused a rapid and lethal cell volume increase to 6206 ± 171 μm^3, which is at the point of cell bursting at the apex. DIDS was further demonstrated to disrupt Cl^- efflux from the apex, indicating that Cl^- flux correlates with pollen tube growth and cell volume status. The signal encoded by inositol 3,4,5,6-tetra*kis*phosphate [Ins(3,4,5,6)P_4] antagonized pollen tube growth, induced cell volume increases, and disrupted Cl^- efflux. Ins(3,4,5,6)P_4 decreased the mean growth rate by 85%, increased the cell volume to 5997 ± 148 μm^3, and disrupted normal Cl^- efflux oscillations. These effects were specific for Ins(3,4,5,6)P_4 and were not mimicked by either Ins(1,3,4,5)P_4 or Ins(1,3,4,5,6)P_5. Growth correlation analysis demonstrated that cycles of Cl^- efflux were coupled to and temporally in phase with cycles of growth. A role for Cl^- flux in the dynamic cellular events during growth is assessed. Differential interference contrast microscopy and kymographic analysis of individual growth cycles revealed that vesicles can advance transiently to within 2 to 4 μm of the apex during the phase of maximally increasing Cl^- efflux, which temporally overlaps the phase of cell elongation during the growth cycle. In summary, these investigations indicate that Cl^- ion dynamics are an important component in the network of events that regulate pollen tube homeostasis and growth.

INTRODUCTION

Pollen tube growth is a prime example of self-organization in biological systems. In these emergent systems, order is achieved by a low number of interactive feedback circuits that control and fine-tune the molecular and biochemical parameters to allow optimum growth and function. Research to identify these feedback circuits in pollen tubes has progressed in recent years and has revealed that growth is organized as a periodic or oscillating system. In light of these results, pollen has become an important and versatile tool for investigations of plant cell development, growth, and biophysics (Taylor and Hepler, 1997; Feijó et al., 2001; Hepler et al., 2001).

Pollen tubes grow by polarized elongation at the apex. This is reflected in the polarized cytological organization: the vegetative nucleus, the generative cell, and larger organelles are located in the distal region of the tube, whereas the apical dome contains mainly small vesicles and endoplasmic reticulum (Pierson and Cresti, 1992). Actin bundles and microtubules extend axially from the pollen grain along the length of the pollen tube to the subapical region, where the overall direction of cytoplasmic flow reverses from anterograde to retrograde (Derksen et al., 1985; Lancelle and Hepler, 1991; Joos et al., 1994; Astrom et al., 1995). The apical

[1] To whom correspondence should be addressed. E-mail zonia@ueb.cas.cz; fax 420-2-33339412.

Article, publication date, and citation information can be found at www.plantcell.org/cgi/doi/10.1105/tpc.003830.

dome contains sparse anastomosing actin filaments (Lancelle and Hepler, 1991; Miller et al., 1996; Kost et al., 1998). Recent work has indicated that periodic elongation of short actin bundles into the apical dome occurs between the growth pulses (Fu et al., 2001). Growth is supported by exocytosis of synthetic materials that are delivered by the highly active vesicle-trafficking system, visualized as cytoplasmic streaming, that transports secretory vesicles along the actin cytoskeleton toward the apical region (Mascarenhas and LaFountain, 1972; Derksen et al., 1995; Miller et al., 1995; Cai et al., 1997; Yokuta et al., 1999). The vesicles accumulate at the region where most actin bundles terminate, near the distal boundary of the apical dome.

The rate of cell elongation at the apex is not linear but oscillates with parameters that are either quasisinusoidal or pulsatory (Tang et al., 1992; Pierson et al., 1995; Geitmann et al., 1996; Geitmann and Cresti, 1998; Feijó, 1999; Feijó et al., 2001). Oscillatory growth is correlated with oscillations in the intracellular concentrations and the extracellular influx of several cations. Of these, Ca^{2+} has been studied most intensively. There is a steep, tip-focused gradient of cytosolic free $[Ca^{2+}]_i$ that has been documented in all species examined (Rathore et al., 1991; Malhó et al., 1994; Pierson et al., 1994; Franklin-Tong et al., 1997). In lily pollen, this gradient decreases from ~10 μM at the tip to 150 to 300 nM at the base 20 μm distal to the tip (Miller et al., 1992; Pierson et al., 1994, 1996; Messerli and Robinson, 1997; Messerli et al., 2000). The $[Ca^{2+}]_i$ gradient oscillation is delayed by ~4 s with respect to growth (Messerli et al., 2000). A further discovery was that Ca^{2+} in the extracellular medium influxes at the apex, also with oscillatory parameters, but with the influx peak delayed by 11 to 15 s with respect to the growth peak (Holdaway-Clarke et al., 1997; Feijó, 1999; Messerli et al., 1999). Oscillatory influx of H^+ and K^+ also has been documented in lily pollen, and these peaks lag behind the growth peaks by ~7 to 11 and 14 s, respectively (Feijó, 1999; Messerli et al., 1999). In lily pollen tubes, H^+ was shown to influx at the tip and efflux at the distal boundary of the apical dome (Feijó et al., 1999). Intracellular H^+ accumulates in a transient, steep gradient at the tip; the $[H^+]_i$ gradient oscillation is delayed by 8 to 10 s with respect to growth (Messerli and Robinson, 1998; Feijó et al., 1999). The distal boundary of the $[H^+]_i$ gradient is marked by an alkaline band whose location correlates with the region of H^+ efflux (Feijó et al., 1999).

The present work is an investigation of Cl^- ion dynamics during pollen tube growth. Anion flux into and out of cells is known to be one of the primary regulators of turgor and intracellular osmotic potential in other plant cells, not only because of its role in salt partitioning during turgor normalization but also because efflux through anion channels depolarizes the membrane (Schroeder and Hedrich, 1989; Ward et al., 1995; Teodoro et al., 1998; Shabala et al., 2000). Indeed, anion flux has been described as "the pacemaker of turgor control" (Sanders and Bethke, 2000). Anions react aggressively with polar water molecules: a rigid layer of six water molecules forms the primary solvation shell, and disruption of this complex has been demonstrated to be energetically unfavorable (Kropman and Bakker, 2001). The primary solvation shell is surrounded by a more loosely associated secondary layer that in turn contacts water molecules with bulk properties. Thus, anions in dynamic aqueous solutions have the potential to influence the ordering of water molecules in a local domain. In light of these considerations, possible correlations between Cl^- flux and cell volume or turgor status in the pollen tube apical region also were examined.

In mammalian secretory cells, Cl^- channels are important regulators of secretory activity and the maintenance of cell volume (Chen et al., 1996). Inositol 3,4,5,6-tetra*kis*phosphate [Ins(3,4,5,6)P_4] has been demonstrated to negatively regulate Ca^{2+}-activated Cl^- channels (Vajanaphanich et al., 1994; Ismailov et al., 1996; Xie et al., 1996, 1998; Barrett et al., 1998; Nilius et al., 1998; Yang et al., 1999; Carew et al., 2000; Ho et al., 2000, 2001). During a screen of a number of different inositol polyphosphates for effects on pollen tube growth, Ins(3,4,5,6)P_4 was identified as a strong effector (L. Zonia, unpublished data). Therefore, potential links between Ins(3,4,5,6)P_4 and Cl^- flux are explored in this study.

The results reported here indicate that oscillatory Cl^- efflux at the pollen tube apex correlates with the cell volume or turgor status within the apical region, is targeted by the signal encoded in Ins(3,4,5,6)P_4, and is temporally coupled to and in phase with growth oscillations. Inspection of dynamic cellular events in the apical region during cycles of growth revealed new information about vesicle movements during cell elongation, and these are discussed in light of a possible role for Cl^- flux oscillations.

RESULTS

Oscillatory Chloride Efflux at the Apex of Tobacco and Lily Pollen Tubes

Noninvasive, ion-specific, vibrating-electrode probe technology was used to measure Cl^- ion flux at the extracellular surface during pollen tube growth. The primary model species in this work was tobacco. During the first 2 to 3 h after the start of germination of tobacco pollen, Cl^- flux at the apex had random fluctuations, but when tube lengths reached 500 to 600 μm, Cl^- efflux became organized into quasisinusoidal, sustained oscillations ($n > 40$) (Figure 1A). Sustained Cl^- efflux oscillations were observed at all subsequent tube lengths examined, from 600 to 1500 μm. Because of the negative charge of the anion, increasing Cl^- efflux was recorded as a negative microvolt potential difference, which led to negative values for the calculated fluxes.

The pollen tube represented by the graph in Figure 1A was growing at a rate of 1.9 μm·min^{-1}, and Cl^- efflux oscil-

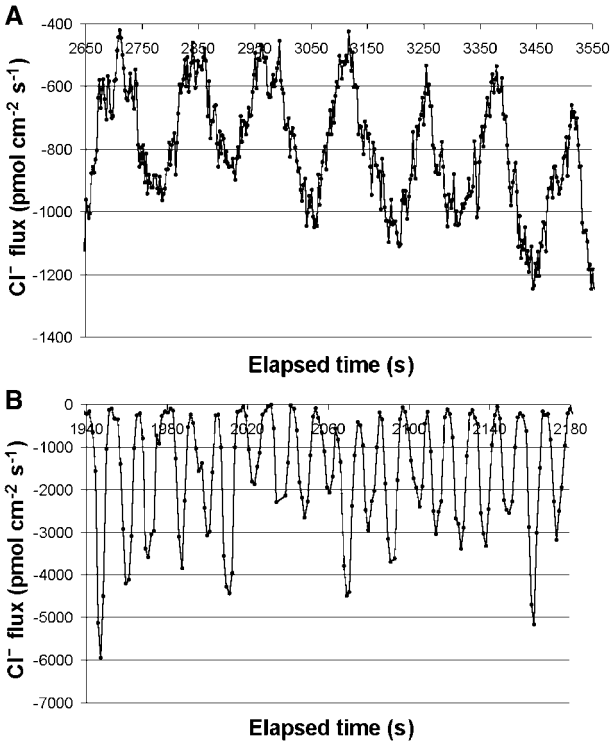

Figure 1. Cl^- Efflux Oscillations at the Apex of Pollen Tubes.

(A) Tobacco.
(B) Lily.

lated with boundary values of 400 to 1200 pmol·cm^{-2}·s^{-1} (which is a threefold increase from the minimum flux value to the maximum flux value during one cycle) and an average period of 105 s. The average Cl^- efflux oscillation periods within populations of pollen were from 50 to 100 s·cycle^{-1}. Values of Cl^- efflux varied by 1 order of magnitude within populations of pollen that had fivefold variations in growth rate values. Tobacco pollen tubes displayed naturally occurring, random, and low-angle curvature during growth that manifested as a migration of the apex focal point within an ~5 μm diameter centered at the tip of the apical dome. During these events, the focal point of Cl^- efflux invariably deployed to the new growth apex concurrent with its migration (data not shown).

To verify and extend the observations of Cl^- efflux oscillations in tobacco pollen, lily pollen tubes also were examined. Short tubes expressed randomly fluctuating Cl^- efflux until reaching a critical length. When the tube length reached 700 to 900 μm, sustained Cl^- efflux oscillations were recorded at the apex (n = 4) (Figure 1B). Cl^- efflux in lily pollen tubes oscillated within boundary values of 50 to 8000 pmol·cm^{-2}·s^{-1}, or a 40- to 160-fold increase from the minimum flux value to the maximum flux value during one cycle. The observed oscillations were very rapid, with an average period of 13.2 s·cycle^{-1}.

Chloride Influx Sites Are Distal to the Subapical Region

To construct a topographical map of Cl^- flux along the pollen tube in regions near the apex, a method was used in which the vibrating microelectrode position is held constant and the pollen tube is allowed to grow past the tip of the microelectrode, thus recording the fluxes along the regional surface of the tube examined. A graph of Cl^- flux in the apical region of a tobacco pollen tube is shown in Figure 2A. These results demonstrate that Cl^- influx occurred at locations distal to the subapical region (Figure 2B). The inversion from oscillatory efflux to net influx started ~12 μm distal to the tip, and influx reached a uniform level starting at 20 to 26 μm distal to the tip.

The Cl^- ion depleted by efflux from the apical pool during each cycle could be refilled readily from the distal sites of Cl^- influx. The spatial coupling of influx and efflux sites predicted that a vectorial flux of Cl^- directed toward the apex would traverse the apical region (Figure 2B). Because the

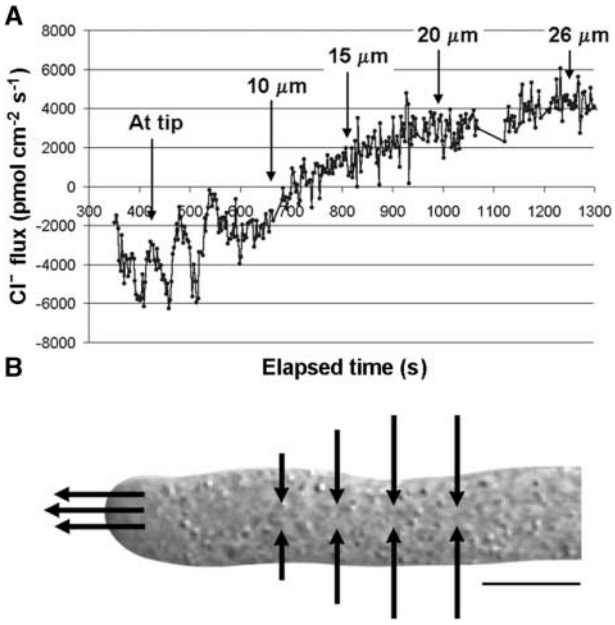

Figure 2. Topographical Mapping of Cl^- Flux along the Cell Surface of the Apical Region.

(A) Profile of Cl^- flux starting at the apex and continuing to 26 μm distal to the tip. There is an inversion of oscillatory efflux to net influx at ~12 μm distal to the tip.
(B) Graphic representation of the vectorial flux of Cl^- into the pollen tube and out from the apex. Bar = 10 μm.

present work is an investigation of the cellular dynamics and function of Cl^- flux, the apical region is defined herein as the length of the pollen tube extending from the apex to 50 μm distal from the tip, which includes both influx and efflux sites.

Chloride Channel Blockers Inhibit Pollen Tube Growth, Induce Cell Volume Increases, and Disrupt Chloride Efflux

Pollen tube growth was inhibited by three different Cl^- channel blockers: 4,4′-diisothiocyanatostilbene-2,2′-disulfonic acid (DIDS), 5-nitro-2-(3-phenylpropylamino)benzoic acid (NPPB), and niflumic acid (Figure 3). For these studies, pollen was cultured for 3 h before addition of the inhibitors and then allowed to grow for another 60 min in the presence of the inhibitors. As shown in Figure 3, the mean growth during 60 min for untreated pollen tubes was 185 μm. Growth was inhibited completely by 20 μM NPPB, 40 μM niflumic acid, and 80 μm DIDS. Cytoplasmic streaming stopped within 10 to 15 min after the addition of 10 μM NPPB and within 10 min after the addition of 20 μM niflumic acid, resulting in the sharp trailing edge of the dose–response curves for these blockers. Cytoplasmic streaming was essentially unaffected by DIDS.

The Cl^- channel blockers also induced increases in apical cell volume. DIDS induced rapid volume increases that were statistically significant at 10 μM ($P = 1.06 \times 10^{-6}$) (Table 1). The apical region underwent a mean cell volume increase from 3905 ± 75 μm^3 in untreated pollen tubes to 6206 ± 171 μm^3 at 80 μM DIDS, and 94% of pollen tubes burst near the apex within 5 to 10 min. Hence, this value represents a mean maximum volume load that is structurally tolerated by the cell.

NPPB and niflumic acid induced cell volume increases that were statistically significant at 5 μM and that reached maxima at 20 μM, the effective dose for growth inhibition for these two blockers (Figure 3). The cell volume increases induced by NPPB and niflumic acid were not as severe as those induced by DIDS; they reached 5613 ± 87 μm^3 and 5223 ± 92 μm^3 at 20 μM NPPB and niflumic acid, respectively. This finding may be attributable in part to the rapid inhibition of cytoplasmic streaming caused by NPPB and niflumic acid, which may reflect the fact that NPPB and niflumic acid target different or additional Cl^- channels than those targeted by DIDS.

DIDS disrupted Cl^- efflux oscillations, as shown in Figure 4. The pretreatment Cl^- efflux is shown in Figure 4A. Within 1 to 2 min after the addition of 10 μM DIDS, the periodic component of the cycle collapsed and the growth rate decreased by 21% (Figure 4B). After another addition of DIDS to a total of 80 μM, Cl^- efflux in this tube was inhibited by ~80% compared with the pretreatment efflux, and there was a cessation of growth; however, this tube did not burst during the recording (Figure 4C).

Together, these results indicate that pollen tube growth and cell volume regulation are linked within a network of circuits that also includes Cl^- efflux.

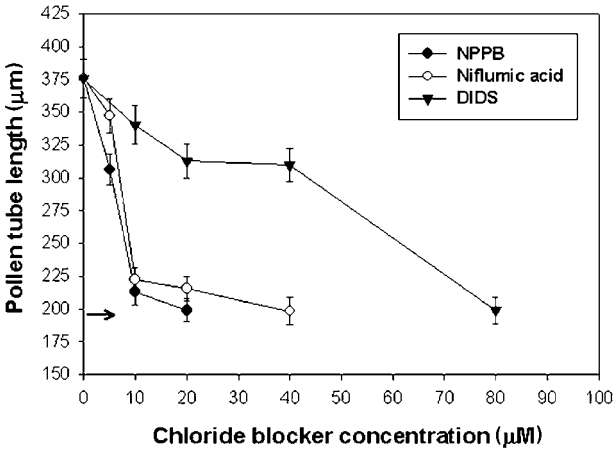

Figure 3. Cl^- Channel Blockers Inhibit Pollen Tube Growth.

Pollen tubes were cultured for 3 h and reached a mean length of 190 μm (arrow) before the addition of channel blockers and further culturing for 60 min. Untreated pollen tubes reached a final mean length of 375 μm. Each value is the mean of 50 pollen tubes ± SE.

$Ins(3,4,5,6)P_4$ Negatively Affects Pollen Tube Growth and Induces Cell Volume Increases

Potential links between the signal encoded in $Ins(3,4,5,6)P_4$ and pollen tube growth were explored. As shown in Table 2, pollen tube growth rate was diminished significantly after microinjection of $Ins(3,4,5,6)P_4$ ($n = 10$). The average growth rate before injection was 3.43 ± 0.29 μm·min^{-1}. After microinjection, the average growth rate decreased to 0.41 ± 0.16 μm·min^{-1} within the first 15 min, but cytoplasmic streaming was either unaffected or recovered fully to preinjection rates within 2 to 4 min. The growth rate of one pollen tube recovered after 15 to 30 min after microinjection (Table 2, line 2), and the growth rate of another was inhibited by ~66% (Table 2, line 5). The growth rates of the remaining eight pollen tubes were inhibited more strongly. The average growth rate at 15 to 30 min after microinjection was 0.53 ± 0.32 μm·min^{-1}. This result is significantly different from the preinjection growth rate ($P = 2.50 \times 10^{-6}$).

The specificity of the negative effect of $Ins(3,4,5,6)P_4$ on growth was demonstrated by microinjection of equivalent concentrations of $Ins(1,3,4,5)P_4$ and $Ins(1,3,4,5,6)P_5$ (Table 2). The average growth rates before and 15 to 30 min after microinjection of $Ins(1,3,4,5)P_4$ were 2.02 ± 0.22 and 2.41 ± 0.18 μm·min^{-1}, respectively ($n = 10$), demonstrating a statistically insignificant stimulation of the growth rate ($P = 0.19$). The average growth rates before and 15 to 30 min after mi-

Table 1. Analysis of Physical Features of the Apical Region of Pollen Tubes Subjected to Different Extracellular Treatments

Experiment[a]	Width (μm)	Area (μm^2)	Volume (μm^3)	Circularity[b]
Untreated Control	9.95 ± 0.09	497.64 ± 4.80	3905.31 ± 74.86	0.4342 ± 0.0027
Chloride Blockers				
DIDS				
10 μm	10.79 ± 0.13	539.55 ± 6.32	4602.29 ± 110.98	0.4577 ± 0.0034
20 μm	11.18 ± 0.10	559.20 ± 5.27	4930.45 ± 91.90	0.4685 ± 0.0027
40 μm	11.94 ± 0.12	597.37 ± 5.96	5628.03 ± 111.86	0.4880 ± 0.0029
80 μm	12.51 ± 0.17	625.80 ± 8.55	6205.79 ± 171.42	0.5014 ± 0.0042
NPPB				
5 μm	11.23 ± 0.11	561.37 ± 5.26	4971.50 ± 93.26	0.4699 ± 0.0028
10 μm	11.71 ± 0.10	585.37 ± 5.17	5402.15 ± 92.40	0.4824 ± 0.0026
20 μm	11.94 ± 0.09	596.95 ± 4.60	5612.80 ± 86.68	0.4884 ± 0.0023
Niflumic acid				
5 μm	11.12 ± 0.09	556.04 ± 4.32	4870.33 ± 76.50	0.4672 ± 0.0023
10 μm	11.45 ± 0.09	572.80 ± 4.69	5170.07 ± 85.02	0.4760 ± 0.0025
20 μm	11.51 ± 0.10	575.56 ± 4.98	5222.59 ± 91.85	0.4774 ± 0.0026
DMSO control[c]	10.00 ± 0.09	500.42 ± 4.54	3947.75 ± 71.34	0.4359 ± 0.0027
Inositol Phosphates				
Ins(3,4,5,6)P_4				
10 μm	10.92 ± 0.11	545.84 ± 5.54	4702.73 ± 95.97	0.4613 ± 0.0031
20 μm	12.31 ± 0.15	615.80 ± 7.80	5997.16 ± 147.74	0.4967 ± 0.0037
Ins(1,3,4,5)P_4				
10 μm	10.38 ± 0.09	518.79 ± 3.78	4244.10 ± 76.43	0.4466 ± 0.0026
20 μm	10.76 ± 0.10	538.41 ± 5.20	4573.35 ± 88.03	0.4574 ± 0.0029
Ins(1,3,4,5,6)P_5				
10 μm	10.30 ± 0.08	515.23 ± 3.78	4178.46 ± 60.27	0.4444 ± 0.0022
20 μm	10.77 ± 0.09	538.77 ± 4.76	4575.09 ± 80.34	0.4576 ± 0.0026
H_2O control[d]				
1% (v/v)	10.33 ± 0.12	516.62 ± 6.01	4222.78 ± 98.84	0.4447 ± 0.0035
2% (v/v)	10.86 ± 0.11	543.37 ± 5.37	4662.09 ± 92.07	0.4598 ± 0.0030

Each value is the mean of 50 pollen tubes ± SE. The region analyzed spans the length of the pollen tubes from the apex extending to 50 μm distal to the tip. Images of the treated pollen tubes were captured within 25 min after the start of treatment for subsequent analysis.

[a] Unpaired *t* test analysis based on volume data indicated that the following sample sets did not differ significantly: untreated control/DMSO control; 10 μm niflumic acid/20 μm niflumic acid. Other samples within each treatment set differed significantly from each other and from the no-treatment control (details given in Results).

[b] The circularity index provided information about pollen tube shape and increases as objects became more spherical.

[c] Chloride blockers were solubilized in DMSO. The volume of DMSO used in this control study represented the maximum volume introduced to the pollen tube cultures, which was equivalent to the amount of solvent for 80 μm DIDS.

[d] Inositol polyphosphates were solubilized in H_2O. The volumes of H_2O introduced to the pollen tube cultures for 10 and 20 μm $InsP_x$ corresponded to 1 and 2% (v/v) H_2O, respectively.

croinjection of Ins(1,3,4,5,6)P_5 were 2.24 ± 0.30 and 2.79 ± 0.41 μm·min^{-1}, respectively (n = 10), demonstrating a statistically insignificant stimulation of the growth rate (P = 0.29).

As a further control for the results of all three inositol polyphosphates, microinjection of an equivalent amount of H_2O was performed (Table 2). H_2O is the solvent in which the inositol polyphosphates were suspended. The average growth rates before and 15 to 30 min after microinjection of H_2O were 3.03 ± 0.29 and 2.35 ± 0.22 μm·min^{-1}, respectively (n = 10), demonstrating a slight decrease in the growth rate (P = 0.08).

It was observed that extracellular addition of Ins(3,4,5,6)P_4 also negatively affected pollen tube growth rate (Table 3). The average growth rate declined from 2.64 ± 0.24 to 0.91 ± 0.18 μm·min^{-1} at 20 μM Ins(3,4,5,6)P_4 (n = 20), which indicates a statistically significant decrease in growth (P = 6.5 × 10^{-7}). Thus, extracellular addition of Ins(3,4,5,6)P_4 inhibited the average growth rate by 66%, whereas intracellular microinjection inhibited the average growth rate by 85%. It is assumed that Ins(3,4,5,6)P_4 added extracellularly is able to interact with its cellular target by crossing the cell wall and membrane.

The specificity of the effect of the extracellular addition of Ins(3,4,5,6)P_4 was demonstrated by the extracellular addition of Ins(1,3,4,5)P_4 and Ins(1,3,4,5,6)P_5 (Table 3). The average growth rates before and after the addition of 20 μM

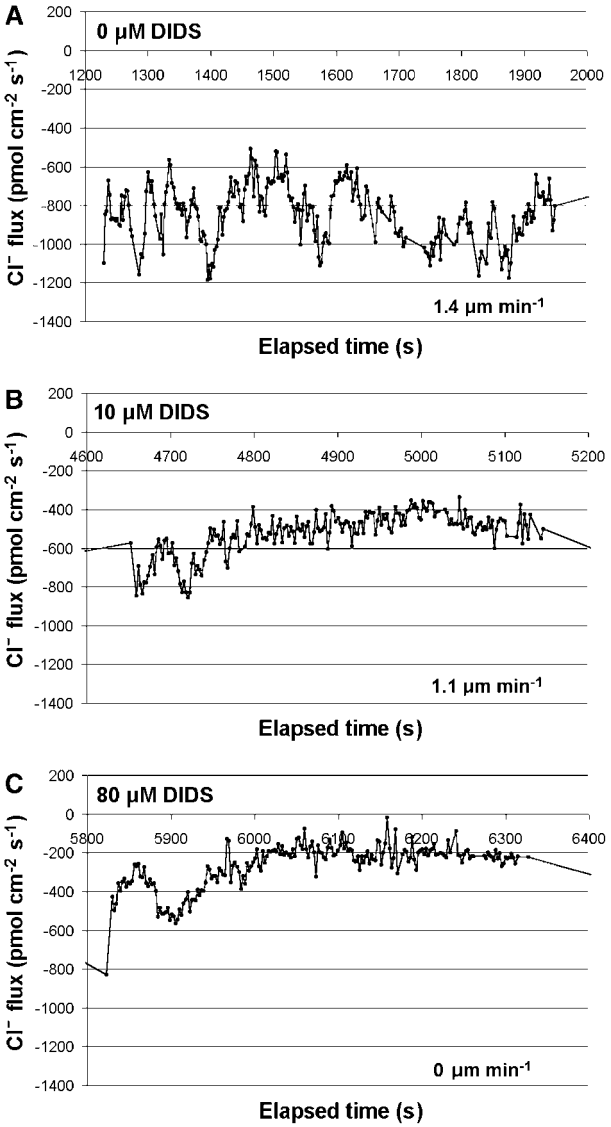

Figure 4. The Cl^- Channel Blocker DIDS Disrupts Cl^- Efflux.

Cl^- efflux oscillations before the addition of DIDS **(A)** and after the addition of DIDS at 10 μM **(B)** and 80 μM **(C)**. Growth rates are given at bottom of each chart.

$Ins(1,3,4,5)P_4$ were 2.42 ± 0.17 and 2.61 ± 0.23 μm·min^{-1}, respectively (n = 20), demonstrating a statistically insignificant difference in the growth rate (P = 0.41). The average growth rates before and after the addition of 20 μM $Ins(1,3,4,5,6)P_5$ were 2.24 ± 0.19 and 2.31 ± 0.31 μm·min^{-1}, respectively (n = 20), demonstrating a statistically insignificant difference in the growth rate (P = 0.83).

For these studies, the growth rate of each pollen tube was measured during a 1.5-min interval, and the entire series of measurements of 20 pollen tubes was completed within 45 min after the start of treatment. However, at treatment times longer than ~45 to 50 min, the average growth rates after the addition of $Ins(1,3,4,5,6)P_5$ also began to decline, possibly as a result of the breakdown of $InsP_5$ to $InsP_4$.

As an additional control for the extracellular effects of the inositol polyphosphates, growth rates also were measured after the addition of equivalent volumes of the solvent H_2O (Table 3). The average growth rates before and after the addition of 2% (v/v) H_2O were 2.68 ± 0.18 and 3.07 ± 0.27 μm·min^{-1}, respectively (n = 20), demonstrating a statistically insignificant increase in the growth rate (P = 0.23). As another control, the growth rates before and after the addition of 2% germination medium were 2.89 ± 0.17 and 3.06 ± 0.14 μm·min^{-1}, respectively (n = 20), demonstrating a statistically insignificant increase in the growth rate (P = 0.47) (data not shown).

Extracellular addition of $Ins(3,4,5,6)P_4$ induced large and rapid increases in apical cell volume (Table 1). The mean cell volume increased from 3905 ± 75 μm^3 for untreated controls to 5997 ± 148 μm^3 at 20 μM $Ins(3,4,5,6)P_4$. This value was on the order of the mean maximum volume load of 6206 ± 171 μm^3 observed with 80 μM DIDS (P = 0.36). This effect on apical cell volume was specific for $Ins(3,4,5,6)P_4$. Addition of 10 and 20 μM $Ins(1,3,4,5)P_4$ and $Ins(1,3,4,5,6)P_5$ caused cell volume increases that were on the order of the cell volume increases after the addition of 1 and 2% H_2O (Table 1). As a further control, apical cell volumes after the addition of 1 and 2% germination medium were 3907 ± 82 and 3890 ± 86 μm^3, respectively (data not shown).

In summary, these data demonstrate that the signal encoded in $Ins(3,4,5,6)P_4$ negatively affected pollen tube growth and rapidly induced large increases in apical cell volume. These effects were specific for $Ins(3,4,5,6)P_4$ and were not mimicked by either $Ins(1,3,4,5)P_4$ or $Ins(1,3,4,5,6)P_5$.

$Ins(3,4,5,6)P_4$ Disrupts Chloride Efflux Oscillations

In addition to negatively affecting pollen tube growth and inducing cell volume increases, $Ins(3,4,5,6)P_4$ disrupted Cl^- efflux from the pollen tube apex (Figure 5). Two different classes of Cl^- flux response to $Ins(3,4,5,6)P_4$ were observed. The first class (n = 11 of 14) had a rapid and essentially complete disruption of Cl^- efflux, whereas the second class (n = 3 of 14) had a transient increase in the peak amplitude and a slight change in the flux periodicity. It is possible that the classes differ in specific functional features such as the homeostatic steady state conditions for anion dynamics or as a result of specific properties of the oscillatory cycles in individual pollen tubes. In both classes, pollen tube growth was disrupted.

The response of the first class of pollen tubes to $Ins(3,4,5,6)P_4$ is shown in Figure 5A. The pretreatment growth rate of this tube was 1.6 μm·min^{-1}. After the addition of 10 μM $Ins(3,4,5,6)P_4$ and a brief lag time for the replace-

Table 2. Microinjection of Ins(3,4,5,6)P_4 Inhibits Pollen Tube Growth

Injectate	Pollen Tube Length (μm)	Distance from Injection Site to Apex (μm)	Growth Rate (μm·min^{-1}) Before Injection	After Injection 0 to 15 min	After Injection 15 to 30 min
Ins(3,4,5,6)P_4	251	90	3.04	0	0.05
	288	110	4.23	0.17	3.23
	312	107	3.08	0.32	0.18
	317	91	3.25	0.02	0.02
	356	130	3.02	1.56	1.02
	364	112	1.85	0.07	0.10
	384	111	3.88	0.65	0
	412	101	5.06	0.08	0.08
	417	102	4.17	0.39	0
	425	116	2.72	0.88	0.61
Ins(1,3,4,5)P_4	236	126	1.59	2.44	2.80
	263	115	1.21	1.83	1.46
	322	118	1.45	1.48	2.27
	370	113	3.34	1.56	2.20
	378	131	1.02	1.46	1.76
	399	101	2.50	1.65	2.50
	428	136	2.19	1.95	2.07
	456	115	2.35	2.15	3.24
	476	99	2.37	1.22	2.91
	492	128	2.22	1.98	2.90
Ins(1,3,4,5,6)P_5	241	91	2.09	1.36	1.91
	286	123	3.62	4.15	5.04
	294	108	2.51	4.65	4.27
	333	106	1.43	1.75	2.38
	340	102	1.10	1.69	1.75
	355	104	3.00	2.53	2.96
	438	103	2.94	2.02	2.77
	446	138	3.20	4.45	4.09
	459	112	1.41	1.89	1.68
	475	117	1.09	1.54	1.05
H_2O	233	131	2.00	1.51	2.11
	267	97	4.78	1.42	3.40
	318	112	2.76	2.28	2.77
	347	89	4.10	1.77	2.51
	362	114	1.88	2.83	2.09
	385	115	3.00	2.10	1.16
	418	105	3.11	1.56	2.12
	428	114	2.78	1.61	1.93
	453	122	2.39	2.06	1.99
	471	128	3.46	2.59	3.44

ment of the vibrating probe, there was evident disruption of Cl^- efflux within 14 min. The pretreatment dynamics of Cl^- flux did not recover within 30 min, the apical region underwent a 25% increase in cell volume, and the growth rate declined.

The response of the second class of pollen tubes to Ins(3,4,5,6)P_4 is shown in Figure 5B. The pretreatment growth rate of this tube was 4.2 μm·min^{-1}. After the addition of 10 μM Ins(3,4,5,6)P_4, the growth rate decreased by 52%, but only slight perturbation of Cl^- efflux occurred. After increasing the concentration to 20 μM Ins(3,4,5,6)P_4, there was another decrease in the growth rate, the apical region underwent a 20% increase in cell volume, and there was a twofold increase in the peak amplitude of Cl^- efflux and a small perturbation of Cl^- efflux periodicity. Some pollen tubes in this class can continue disordered Cl^- efflux at a low and chaotic rate for several hours after exposure to Ins(3,4,5,6)P_4. The resultant new growth regions generally were highly aberrant, with distorted or twisted tube tips.

Together, these results indicate that the signal encoded in Ins(3,4,5,6)P_4 can act in regulatory networks that target pollen tube growth, cell volume regulation, and Cl^- efflux.

The Periodicity of Chloride Efflux Is Temporally in Phase with Growth Periodicity

Correlation analyses were performed to simultaneously record Cl^- efflux and measure pollen tube growth rate to determine the temporal relationship between the two oscillations. The Cl^- efflux values were converted from microvolt differential recordings (negative values) to absolute flux (positive values) to plot correlations. Sequential images of the pollen tube apical region were captured during 5- to 10-min growth sequences, and the position of the tip boundary was tracked using a subpixel-resolution pattern identification function. The coordinates corresponding to the position of the tip boundary were transformed to a velocity function, exported to a spreadsheet, and plotted. The growth rate curve was plotted with the Cl^- efflux oscillation curve using the time axis, and the temporal relationship was determined.

As shown in Figure 6, Cl^- efflux peaks were coupled closely with growth rate peaks: sometimes slightly preceding (single arrows), sometimes overlapping (double arrow), and sometimes slightly delayed (triple arrow). In this sequence, the first Cl^- efflux cycle was broad and had two shoulders (asterisks) that overlapped simultaneous shoulders in the first broad growth cycle. Globally, cycles of Cl^- efflux preceded cycles of growth by 0.25 ± 0.5 s (n = 22 peaks from five independent experiments). However, the temporal resolution for Cl^- flux recording was on the order of 1.5 to 2 s. Thus, for technical reasons, Cl^- efflux oscillations and growth rate oscillations should be considered to be temporally coupled in phase.

Chloride Efflux Correlates with Vesicle Movement during the Growth Cycle

Because cycles of Cl^- efflux and growth were coupled and in phase, investigations were performed to determine a role for Cl^- efflux in the physical processes that mediate growth. These studies required the correlation of multiple dynamic events that differ in the resolution limits that can be achieved with the technologies used and that are required

Table 3. Addition of Ins(3,4,5,6)P_4 Inhibits Pollen Tube Growth

Solution	Mean Growth Rate ($\mu m \cdot min^{-1}$)
Ins(3,4,5,6)P_4	
0 μm	2.64 ± 0.24 (1.06, 4.78)
10 μm	1.14 ± 0.19 (0, 2.99)
20 μm	0.91 ± 0.18 (0, 3.26)
Ins(1,3,4,5)P_4	
0 μm	2.42 ± 0.17 (1.07, 4.51)
10 μm	2.68 ± 0.18 (1.34, 5.10)
20 μm	2.61 ± 0.23 (0.76, 5.93)
Ins(1,3,4,5,6)P_5	
0 μm	2.24 ± 0.19 (1.14, 3.79)
10 μm	2.65 ± 0.26 (1.10, 5.43)
20 μm	2.31 ± 0.31 (0.48, 6.09)
H_2O	
0% (v/v)	2.68 ± 0.18 (1.44, 4.96)
1% (v/v)	3.05 ± 0.22 (1.63, 6.46)
2% (v/v)	3.07 ± 0.27 (0.90, 5.10)

Each value is the mean growth rate of 20 pollen tubes ± SE, with minimum and maximum values given in parentheses.

for the optimization of the analyses. To reach the goal, a two-step approach was used.

The first step was to optimize the correlation between Cl^- efflux cycles and dynamic events that occur in the apical region during growth. Pollen tube growth was imaged using differential interference contrast (DIC) microscopy simultaneously with recording of Cl^- efflux (Figure 7A). To allow continuous monitoring of the microelectrode position, images were captured at 1 s·image^{-1}. For these studies, the imaging tool of kymographic analysis was used (Figure 7B). The image area analyzed for the kymograph is shown in Figure 7C as the transect between the two outer green lines. The kymograph allowed the analysis of dynamic changes in the average refringence of this enlarged transect. The average pixel intensity along the transect was compressed to a thin line, and a color-coded look-up table was used to highlight differences in intensities. The transects were aligned subsequently with respect to the apical cell wall position, so the length of cell elongation during growth appears as the distal extension of the kymograph. Alignment of the transects in a temporal sequence gives the time-lapse kymograph shown in Figure 7B.

Before the phase of Cl^- efflux from the apex (0 to 10 s), the distal boundary of the clear zone (light blue) in this cell was ~7 μm from the wall boundary. During the phase of maximally increasing Cl^- efflux from the apex (30 to 60 s), there was an average advance of vesicles and small organelles (dark blue-green and yellow) into the apical dome to within 3 to 4 μm from the pollen wall. This advance may be interpreted as a dynamic sum of the number of vesicles and organelles located in or near the apical dome times the frequency of movement into the apical dome. The original boundary of the clear zone was reestablished after the growth pulse (70 to 80 s). Although Cl^- efflux preceded growth during this cycle (Figure 7A), the kymograph shows overlap between the events (Figure 7B). In light of the time resolution that can be achieved and the required degree of processing, these results led to the interpretation that Cl^- efflux, vesicle advance into the apical dome, and growth probably all occurred essentially in phase.

The second step was to optimize the correlation of cytoplasmic dynamics with cycles of growth. For these studies, high-definition DIC microscopy was used, and images were captured at a rate of 0.21 s·image^{-1}. The results of these studies are presented in Figure 8, which illustrates two cycles of growth (Figure 8A). Before the growth pulse, there was a well-defined clear zone in the apical dome that was essentially free of larger vesicles and organelles (Figure 8B; 223.0 and 331.7 s). During the phase of the cycle with maximally increasing growth rate, vesicles and small organelles advanced transiently into the apical dome to within 2 to 3 μm of the apical plasma membrane (Figure 8B; 281.7 and

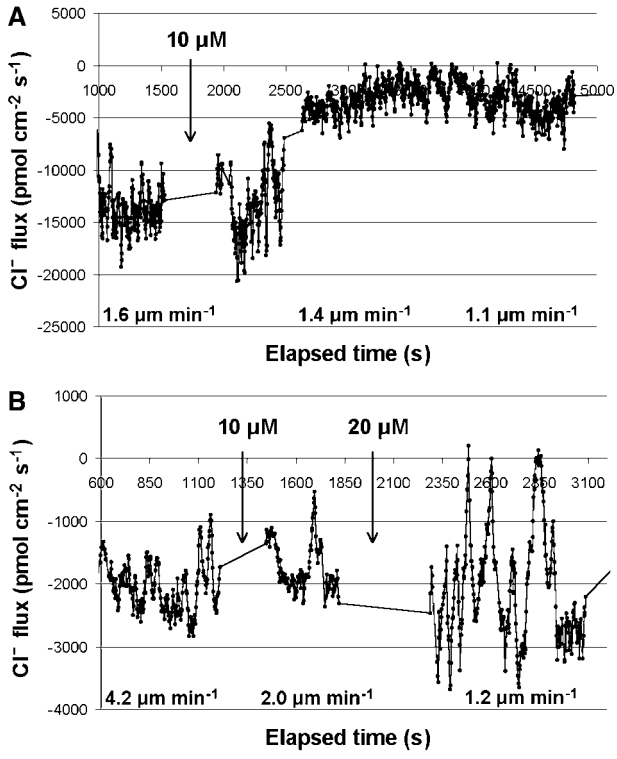

Figure 5. Ins(3,4,5,6)P_4 Disrupts Cl^- Efflux at the Pollen Tube Apex.

(A) Cl^- efflux profile of class I tobacco pollen tubes before and after the addition of 10 μM Ins(3,4,5,6)P_4 (arrow).

(B) Cl^- efflux profile of class II tobacco pollen tubes before and after the addition of 10 and 20 μM Ins(3,4,5,6)P_4 (arrows).

Growth rates are given at bottom of each chart.

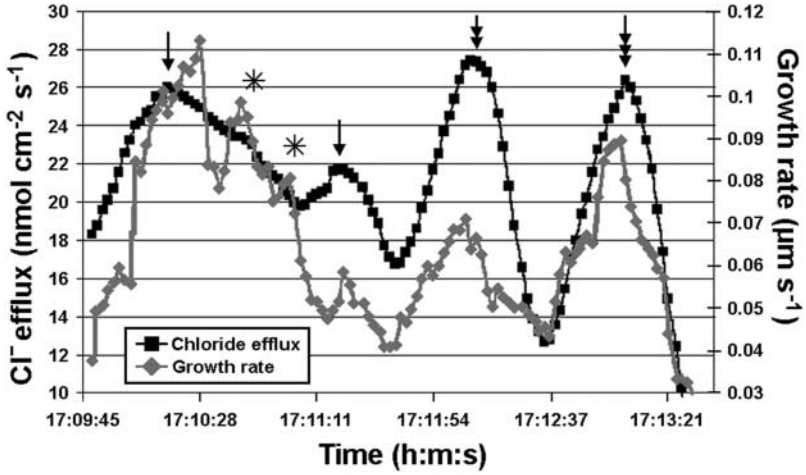

Figure 6. Correlation of Growth Rate Oscillations with Cl^- Efflux Oscillations in Tobacco Pollen Tubes.

The global average indicates that Cl^- efflux and growth peaks are temporally coupled and in phase. Gray symbols, growth rate oscillations; black symbols, Cl^- efflux oscillations. Single arrows indicate Cl^- efflux peaks slightly preceding growth rate peaks; the double arrow indicates Cl^- efflux peaks overlapping growth rate peaks; the triple arrow indicates Cl^- efflux peaks slightly delayed after growth rate peaks. The asterisks indicate the two shoulders of the first Cl^- efflux cycle.

387.8 s). This event occurred during the phase of the cycle with maximally increasing Cl^- efflux from the apex (Figures 6 and 7). When growth rates and Cl^- efflux rates reached steady maxima, the distance between the apex and the location of vesicles and organelles increased (Figure 8B; 303.8 and 410.5 s). At the end of the cycle, the clear zone in the apical dome was reestablished, as can be observed in the transition that occurred from 303.8 to 331.7 s (Figure 8B). Together, these results indicate that during the phase of the cycle with maximally increasing growth rate, a transient forward movement or flow of vesicles into the apical dome can occur. In conjunction with the results shown in Figures 6 and 7, it is proposed that Cl^- efflux out of the apex correlates with this forward flow of vesicles and organelles during cell elongation.

DISCUSSION

Chloride Flux, Cell Volume Regulation, and Pollen Tube Growth Oscillations

These studies have identified a new ion circuit in pollen tubes, have demonstrated that Cl^- flux is required for growth, have documented a role for Cl^- flux in the maintenance of cell volume, have explored potential links between Cl^- flux and inositol polyphosphate signals, and have investigated correlations between Cl^- flux and the dynamic events that mediate cell elongation. In light of the fact that oscillatory Cl^- efflux has been found to be coupled in phase with oscillatory growth, this circuit appears to have important roles within the network of events that regulate pollen tube growth and homeostasis.

Cl^- flux is necessary for pollen tube growth. Blocking Cl^- flux with Cl^- channel blockers rapidly inhibited growth (Figures 3 and 4), and modulation of the level of Cl^- that moves across the plasma membrane had a role in maintaining cellular homeostasis (Table 1). Individual pollen tubes from heterogeneous populations had varying levels of Cl^- efflux. This may reflect differences in the number or distribution of channels in the apical plasma membrane, which could lead to large variations in ion flux per unit of plasma membrane. However, the frequency of Cl^- efflux was coupled tightly to growth (Figure 6). Nonlinear signals can carry information encoded in the signal amplitude and the signal frequency (Allen et al., 2000, 2001). Recent analyses indicate that the frequency of the Cl^- efflux signal is uniform across populations of tobacco pollen that have normal growth dynamics, so it may be important in regulating pollen tube growth (L. Zonia, unpublished data).

A second role for Cl^- flux is in regulating cell volume or turgor pressure. Inhibition of Cl^- flux rapidly induced increases in apical cell volume (Figure 3, Table 1). Cell volume increased to critical levels at 80 μM DIDS, at which point 94% of the pollen tubes burst within 5 to 10 min. The critical point at which bursting occurred represents a 58.9% volume increase along the apical 50-μm length of the tube. The fact that this lethal increase occurred within 5 to 10 min suggests that a dynamic flux of H_2O may traverse the pollen tube apical region. Rapid and large cell volume increases

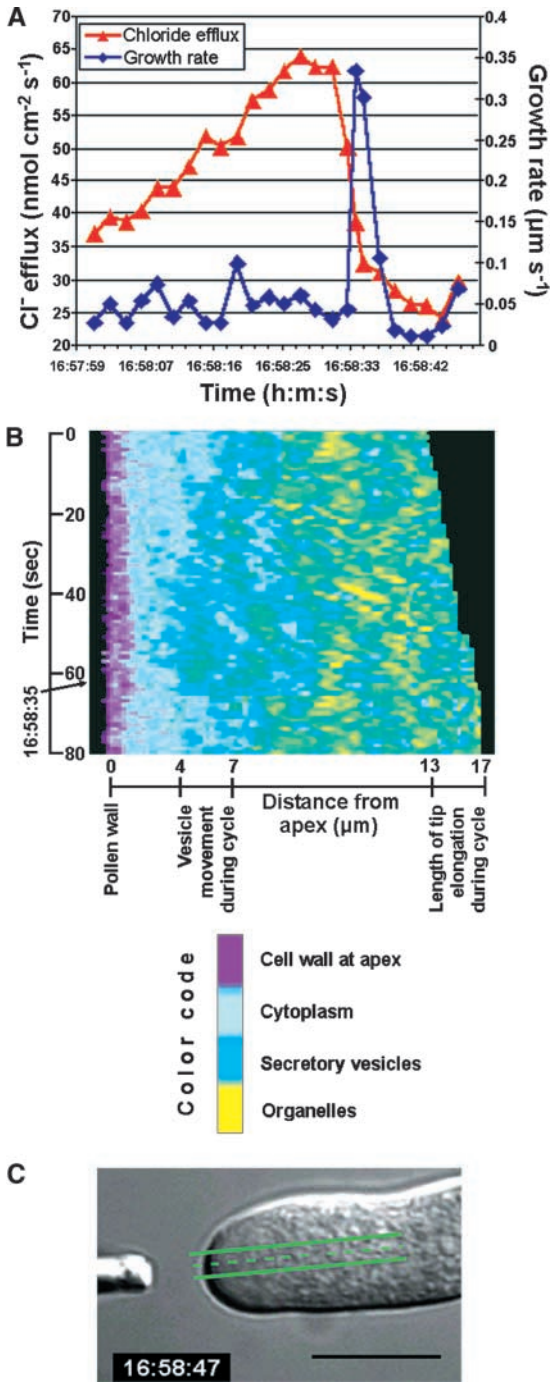

Figure 7. Correlation of Cl^- Efflux and Cytological Changes in the Apical Region during One Growth Cycle of a Tobacco Pollen Tube.

(A) Temporal relationship of the Cl^- efflux peak (red symbols) with the growth peak (blue symbols).

(B) Kymogram showing the average position of vesicle and organelle movement during the cycle. Distance from the apex is marked along the *x* axis, and elapsed time during the cycle is marked along the *y* axis. The color scale key for the kymogram is given at bottom.

(C) Image representing the origin of the kymogram. A transect of 30 pixels wide between the green lines was extracted from the time-stamped stacked images, a color-coded look-up table was applied to the average refringence along the transect, and transects were aligned by normalizing the apex boundary to construct the kymogram shown in **(B)**. Bar = 10 μm.

also were induced by Ins(3,4,5,6)P_4 (Table 1). Thus, the evidence indicates that agents that perturb Cl^- flux also perturb pollen tube turgor pressure. This finding suggests a close correlation between Cl^- efflux and the regulation of pollen tube osmotic balance or hydrodynamics. Anion channels are known to function in the regulation of hydrodynamics in other plant cells (see below). Cl^- efflux may be linked within a network of circuits that are activated upon changes in turgor status, including plasma membrane stretch-sensitive Ca^{2+} channels (Hedrich et al., 1990; Takahashi et al., 1997; Taylor et al., 1997, Goddard et al., 2000) and stretch-sensitive Cl^- conductances (Cosgrove and Hedrich, 1991). A coordinated network including single-channel stretch-sensitive Cl^- flux in concert with stretch-sensitive Ca^{2+}-activated Cl^- flux may provide the necessary levels of feedback to fine-tune and control the pollen tube osmotic balance under variable extracellular conditions.

A third role for Cl^- flux is correlated with the dynamic properties of pollen tube growth. During the growth pulse, the apical Cl^- pool would be depleted by efflux through the apex, and this would be refilled readily by the distal Cl^- influx pool (Figure 2A). This effect results in a Cl^- anion circuit that traverses the pollen tube apical region and fluxes out through the apex (Figure 2B). This vectorial flux of Cl^- through the apical region may provide part of the driving force for the transient forward movement of vesicles and organelles and for cell elongation (Figures 7 and 8), perhaps via an entrained hydrodynamic flow (Zonia et al., 2001).

One key to understanding how pollen tubes grow lies in understanding the temporal relationship among the ion circuits with respect to the start of the growth pulse. Oscillatory Cl^- efflux is coupled temporally to and in phase with the start of the growth pulse (Figure 6). In lily pollen tubes, the next event, an increase in the cytosolic Ca^{2+} gradient, occurs 4 s after the start of the growth pulse (Messerli et al., 2000). It is not known where the Ca^{2+} that initiates this cytosolic increase originates from, but entry of extracellular Ca^{2+} through stretch-sensitive channels has been postulated. The start of the growth cycle in tobacco pollen tubes is sometimes preceded by a sharp and transient forward surge of the tip boundary position. Together, these observations suggest the activation of stretch-sensitive Ca^{2+} and Cl^- channels in concert with Cl^- efflux in stimulating the onset of the growth cycle.

Anion Channels Have Roles in Turgor Regulation and Cellular Signaling

Anion flux has been recognized as an important early component of both plant and animal cell responses to specific signal transduction cascades (Marten et al., 1991; Schroeder, 1995; Ward et al., 1995; Barbier-Brygoo et al., 2000; Schroeder et al., 2001). Two plant organs are known to use a strategy of controlled hydrodynamics in the form of reversible cell swelling to perform work: stomatal guard cells, which open upon swelling and allow gas exchange for photosynthesis to occur (Assmann, 1993), and pulvinar extensor cells, which control leaflet opening in *Samanea* (Satter et al., 1988). The cell volume changes in both systems are driven primarily by dynamic ion fluxes (Schroeder and Hedrich, 1989; Liu and Luan, 1998).

In guard cells, it has been shown that light activates the plasma membrane H^+-ATPase, which leads to membrane hyperpolarization (Assmann et al., 1985; Amodeo et al., 1992) and ultimately results in passive uptake of K^+ and in some species Cl^-. This leads to the movement of H_2O into the cell along its osmotic potential gradient and stomatal opening. This process is reversed by the inhibition of H^+-ATPase and the opening of Cl^- efflux channels, which depolarizes the membrane and leads to passive efflux of K^+ out of the cell and subsequent decreases in cell volume (Schroeder and Hedrich, 1989; Ward et al., 1995). Studies of osmoregulation in other plant cells have focused on events induced by hyperosmotic conditions, and turgor normalization has been associated with decreased efflux of Cl^- (Teodoro et al., 1998) or increased influx of Cl^- and K^+ (Shabala et al., 2000).

Targets of Signal Transduction Cascades Mediate Cyclic Behaviors, Ion Dynamics, Growth, and Cellular Homeostasis

Inositol phospholipid and inositol polyphosphate signal transduction cascades initiate and integrate complex cellular behaviors and responses to specific stimuli. Of particular interest for the present context, recent work has demonstrated that oscillatory Ca^{2+} spiking in cultured rat cardiac cells is controlled by the concerted activity of a cluster of kinases that includes phosphatidylinositol 3-kinase and phospholipase C (Bony et al., 2001). The tightly regulated activity of these interconnected kinase networks ultimately results in oscillations in the levels of Ins(1,4,5)P_3, which in turn mobilize the spiking Ca^{2+} oscillations. This demonstration of a mechanism to drive rapid oscillations in the levels of Ins(1,4,5)P_3 is interesting for the present study, which indicates potential links between Ins(3,4,5,6)P_4 signaling and Cl^- efflux oscillations.

Evidence for the importance of inositol phospholipids and inositol polyphosphates in plant cells is accumulating (for reviews, see Munnik et al., 1998; Drøbak et al., 1999;

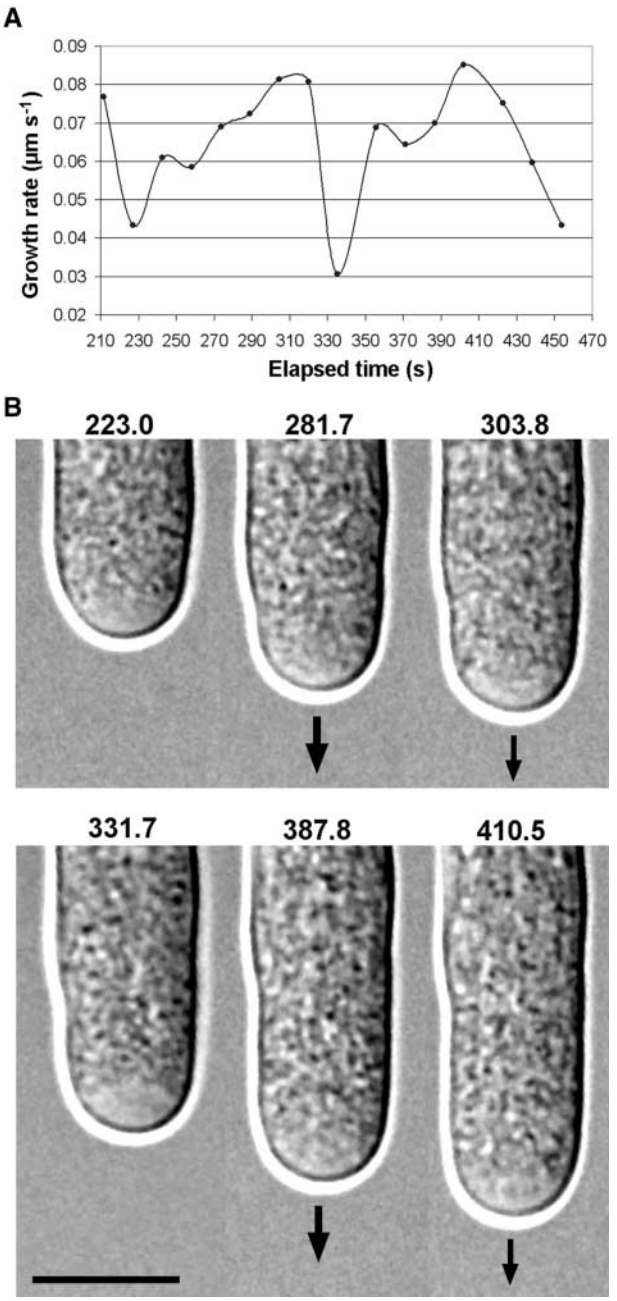

Figure 8. Time-Lapse DIC Imaging of Cellular Dynamics during Two Growth Cycles.

(A) Growth rate oscillations during two growth cycles.
(B) Time-lapse images of the apical region. The distal edge of each image has been normalized to the same reference point. Elapsed times in seconds are given above each image and correspond with the elapsed times given in the growth rate chart shown in **(A)**. Cl^- efflux is represented by the vectors at the tube tip. Bar = 10 μm.

Stevenson et al., 2000; Munnik and Meijer, 2001). Hyperosmotic stress was shown to induce the synthesis of phosphatidylinositol 3,5-bisphosphate [PtdIns(3,5)P_2] in pea, tomato, and alfalfa cells (Meijer et al., 1999), whereas in Arabidopsis cells, PtdIns(4,5)P_2 was observed to accumulate (Pical et al., 1999). Much attention in plant research has focused on the signaling role of Ins(1,4,5)P_3, which mobilizes the release of intracellular Ca^{2+}. Photolysis of caged Ins(1,4,5)P_3 injected into pollen tubes has been shown to cause an increase in free Ca^{2+}, with the greatest increase observed in the region of the vegetative nucleus (Franklin-Tong et al., 1996; Malhó, 1998). Further studies have demonstrated a role for PtdIns(4,5)P_2 in conjunction with the small G-protein Rac at the tip of Arabidopsis pollen tubes during elongation (Kost et al., 1999).

Functional roles for other inositol polyphosphates are emerging (for reviews, see Mennitti et al., 1993; Shears, 1996; Caffrey et al., 1999; Irvine and Schell, 2001). One of these isomers is Ins(3,4,5,6)P_4, which has been shown to negatively regulate a Ca^{2+}-activated Cl^- channel that is important for secretion and osmoregulation in epithelial secretory cells (Vajanaphanich et al., 1994; Ismailov et al., 1996; Xie et al., 1996, 1998; Barrett et al., 1998; Nilius et al., 1998; Yang et al., 1999; Carew et al., 2000; Ho et al., 2000, 2001). Ins(3,4,5,6)P_4 has been identified in the duckweed *Spirodela* (Brearley and Hanke, 1996), and Ins(3,4,5,6)P_4 1-kinase and 4- and 6-phosphatase activities have been detected in *Commelina* mesophyll cells (Brearley and Hanke, 2000).

This report has demonstrated that Ins(3,4,5,6)P_4 can act in regulatory circuits that target pollen tube growth, cell volume regulation, and Cl^- flux (Tables 1 to 3, Figure 5). The effects on growth and homeostasis are not mimicked by either Ins(1,3,4,5)P_4 or Ins(1,3,4,5,6)P_5. The 1-hydroxyl group appears to be essential for binding and inhibition of the Cl^- channel, whereas the 2-hydroxyl group plays a less essential role (Rudolf et al., 1998). Levels of Ins(3,4,5,6)P_4 in animal cells increase slowly after stimulus-dependent hydrolysis of PtdIns(4,5)P_2 to Ins(1,4,5)P_3 (Stephens et al., 1988; Balla et al., 1989). In unstimulated cells, the concentration of Ins(3,4,5,6)P_4 is estimated to be ~1 μM and increases to 10 to 15 μM upon cell activation (Pittet et al., 1989; Vajanaphanich et al., 1994). Two immediate precursors of Ins(3,4,5,6)P_4 have been reported: Ins(3,4,6)P_3 and Ins(1,3,4,5,6)P_5. Whether one or both of these precursors represent functional pathways in various cell types undergoing different developmental processes is a matter of investigation.

In both plants and animals, Ins(3,4,5,6)P_4 is phosphorylated to Ins(1,3,4,5,6)P_5 and InsP_6 by sequential 1-kinase and 2-kinase activities. InsP_6 has been shown to inhibit an inward-rectifying K^+ current in patch-clamp studies of guard cells (Lemtiri-Chlieh et al., 2000). This inhibition is Ca^{2+} dependent, and the evidence indicates that it is elicited after treatment with abscisic acid that induces cell volume decreases leading to stomatal closure (Lemtiri-Chlieh et al., 2000). The present report has shown that Ins(3,4,5,6)P_4 antagonizes Cl^- efflux from the pollen tube apex (Figure 5), disrupts pollen tube growth (Tables 2 and 3), and induces rapid and large cell volume increases (Table 1). Together, these recent investigations of inositol polyphosphate signaling in plants present the intriguing results that Ins(3,4,5,6)P_4 and InsP_6—which are linked by phosphorylation cycles through an Ins(1,3,4,5,6)P_5 intermediate—target ion channels that have antagonistic functions in regulating plant cell osmotic potential.

METHODS

Pollen Culture

For experiments to measure Cl^- fluxes, pollen from tobacco (*Nicotiana tabacum* cv Samsun) was germinated as follows. Pollen was removed from −20°C, and after 25 to 30 min at room temperature, the appropriate mass of pollen to give a final culture density of 0.06 mg·mL^{-1} was dispersed in germination medium in plastic Petri dishes. Germination medium consisted of 6% Suc, 1.6 mM H_3BO_3, 200 μM $CaCl_2$, and 25 μM MES, pH 5.5. Cultures were placed on a rotary shaker at 100 rpm and were allowed to germinate and grow at 23°C for 3 to 7 h. The cultures were used directly in the Petri dishes in which they had been germinated and were not divided into aliquots before recording of Cl^- flux to avoid mechanical perturbation of the cells. Under the culture conditions used, >80% of the pollen tubes had oscillatory growth, with rates from 1.3 to 4.5 μm·min^{-1}.

To measure Cl^- flux in lily (*Lilium longiflorum*), pollen was removed from −70°C and placed in a humid chamber at room temperature for 1 h before sowing a small amount on germination medium in a plastic Petri dish. Germination medium consisted of 5% Suc, 1.0 mM KCl, 50 μM $CaCl_2$, 1.6 mM H_3BO_3, and 50 μM Mes, pH 5.5. Cultures were placed on a rotary shaker at 100 rpm and were allowed to germinate and grow at 23°C for 3 to 6 h.

Chloride Blocker Studies

The Cl^- blockers included 4,4′-diisothiocyanatostilbene-2,2′-disulfonic acid (DIDS) and niflumic acid, both from Sigma (St. Louis, MO), and 5-nitro-2-(3-phenylpropylamino)benzoic acid (NPPB) from TOCRIS (Bristol, UK). Tobacco pollen was germinated as described above except that culture densities were increased to 1 mg·mL^{-1}. Pollen was germinated and grown for 3 h, at which time the Cl^- blockers were added to individual cultures simultaneously with stopping of untreated control cultures by the addition of a fixative solution at 1:1 (v/v). The fixative solution contained glycerol:glacial acetic acid:H_2O at 2:1:1. Untreated control cultures and cultures treated with Cl^- blockers were allowed to continue growing for another 60 min before stopping of all cultures by the addition of fixative solution. Then, the lengths of 50 pollen tubes were measured for each sample using the calibrated measuring function of Lucia Image Analysis version 3.5 (Laboratory Imaging, Prague, Czech Republic). All tests were performed in duplicate, and experiments were repeated three times.

To investigate the effect of the Cl^- blockers on Cl^- efflux, control studies were performed to assess the effect of DIDS, NPPB, and niflumic acid on the ionophore cocktail of the microelectrodes. It was

found that only DIDS did not significantly affect the voltage recordings of the microelectrodes (data not shown), so DIDS was selected for further studies.

Measurement of Physical Features of the Pollen Tube Apical Region

Pollen was germinated as described above except that the density was increased to 0.4 mg·mL^{-1} and cultures were grown in glass Petri dishes. Pollen was allowed to germinate and grow for 3.5 to 4.5 h before the experiments were started. The reagent of interest was added to the cultures and mixed by gentle swirling, and images of the pollen tube apical regions were captured starting at 5 min after the addition. Imaging was performed with a Nikon Eclipse 600 upright microscope (Tokyo, Japan) with a 40×0.6 PlanApo extra-long-working-distance objective and a high-performance charge-coupled device (CCD) camera (Cohu, Poway, CA).

Images were captured using Lucia Image Analysis version 3.5 (Laboratory Imaging); 50 images for each experiment were captured within 25 min after the start of treatment. Images were analyzed using the Lucia calibrated measurement functions. Each experiment was repeated twice, and the reported values were typical for both experiments. To trace pollen tube perimeters, a measurement frame was chosen that selected the clearly defined boundary of the plasma membrane with a length extending to 50 ± 0.5 μm distal to the tip.

Area is the principal measurement determined because calibration of the objective provides a direct scaling relationship with the number of pixels selected in the measurement frame. Width (W) then was calculated as

$$W = \frac{A}{L},$$

where A is the area and L is the length. The volume (V) calculation is based on an equivalent right circular cylinder, with radius defined as 0.5 × W and height defined as the length: $V = \pi (0.5 \times W)^2 \times L$. Circularity (C) provides information about the pollen tube shape and is calculated from the area and the perimeter (P):

$$C = \frac{4\pi A}{P^2}.$$

The perimeter is the total boundary measure and is calculated from four projections in the directions 0, 45, 90, and 135° using Crofton's formula: $P = \pi\ 0.25 \times (P_0 + P_{45} + P_{90} + P_{135})$.

Chloride Flux Measurements

An ion-selective vibrating electrode (Kühtreiber and Jaffe, 1990; Kochian et al., 1992; Shipley and Feijó, 1999) was used to measure extracellular Cl^- flux in pollen tubes. Electrodes were pulled from 1.5-mm borosilicate glass capillaries (World Precision Instruments, Sarasota, FL) with a Sutter P-98 Flaming Brown electrode puller (Sutter Instruments, Novato, CA). These were then baked in covered dishes at 250°C for 8 to 12 h and vaporized with dimethyl dichlorosilane (Sigma) for 30 min, and the covers were removed before further baking at 250°C for 1 h.

Electrodes were constructed as follows. The capillaries were backfilled with a 15- to 20-μm column of 100 mM KCl and then front-loaded with a 20- to 25-μm column of Cl^--selective liquid exchange cocktail (number 24899; Fluka, Milwaukee, WI). An Ag/AgCl wire electrode holder (World Precision Instruments) was inserted into the back of the electrode and established electrical contact with the bathing solution. A dry reference electrode (World Precision Instruments) was inserted into the sample bath. Signals were measured with a custom-built electrometer (Applicable Electronics, Forestdale, MA).

Electrode vibration and positioning were achieved with a stepper-motor-driven three-dimensional positioner. Data acquisition, preliminary processing, control of the three-dimensional electrode positioner, and stepper-motor-controlled fine focus of the microscope stage were performed with ASET software (Science Wares [East Falmouth, MA] and Applicable Electronics). The self-referencing vibrating probe oscillates with an excursion distance of 10 μm. A typical cycle was completed in 2.33 s; each cycle includes an adjustable settling time after each move, one measuring period at each extreme of the cycle, and the excursion time. The measurement taken nearest to the cell is subtracted from the measurement taken at the opposite end of the cycle. This subtraction represents the self-referencing feature of the probe.

Cl^- flux at the surface of a pollen tube was measured by vibrating the electrode tip within 5 μm of the tube. Background references were taken at more than 1 mm from any pollen grain or tube, and the values were subtracted from the microvolt differential recordings during data processing using Microsoft Excel version 4.0. During the initial stages of developing and optimizing methods for the measurement of Cl^- flux, the integrity of the liquid exchange cocktail was examined and found to have a dynamic response for Cl^- that is ≥3 orders of magnitude better than that for other anions tested. An anion secreted by pollen tubes could affect the background recording and lead to an overestimation of Cl^- flux. This was controlled by determining the levels of Cl^- in pollen cultures at different times after the start of germination using the Microquant assay kit from Merck (Darmstadt, Germany). This assay is based on the reaction of Cl^- with mercuric thiocyanate in the presence of ferric iron to produce mercuric chloride and ferric thiocyanate. The final reaction color is linearly dependent on the initial Cl^- concentration. These results gave values of Cl^- concentration that fell within an acceptable range of the background recordings collected during the experiments.

The vibrating-electrode system was attached to a Nikon Eclipse TE-300 inverted microscope that was housed inside a copper-sheet Faraday cage supported on a vibration-free platform. For routine experiments, a ×20 PlanApo objective under differential interference contrast (DIC) was used. For growth correlations, most sequences were obtained with a 60×1.4 PlanApo or a 100×1.3 PlanFluo objective, both oil immersion and under DIC optics.

Pharmacological studies and hypoosmotic treatments were performed in the following way. A pretreatment efflux pattern was ascertained for a minimum of 15 min. Data collection was halted, the Faraday cage was opened, and a predetermined volume of the agent of interest was disbursed carefully to the culture medium. The Faraday cage was closed, the electrode was repositioned next to the tip, and data collection was resumed.

Inositol Polyphosphate Studies

Inositol 3,4,5,6-tetra*kis*phosphate [Ins(3,4,5,6)P_4] and Ins(1,3,4,5,6)P_5 were synthesized by Matreya Inc. (Pleasant Gap, PA) and obtained through BioTrend Chemikalien (Köln, Germany). Ins(1,3,4,5)P_4 was from Sigma. Microinjection studies were performed as follows. A semirigid substratum consisting of 5.5% (w/v) low-gelling-temperature

agarose (type VII; Sigma) in germination medium was spread on the surface of a microscope slide and allowed to gel before overlaying with 400 μL of a 2 mg·mL^{-1} suspension of pollen in germination medium. Pollen was allowed to germinate and grow in a humid chamber for a minimum of 3 to 4 h and a maximum of 7 h.

Before beginning the experiments, excess medium was carefully removed from the agarose slab. During the time that the slide was on the microscope stage, germination medium was added periodically along the edges of the agarose slab to keep the pollen tubes hydrated. Microinjection was performed on a Nikon Eclipse 600 upright microscope with a 40×0.6 PlanApo extra-long-working-distance objective and a Narashige 4-D hydraulic micropositioner and pressure injector (Tokyo, Japan). Microinjection needles were pulled from 1.0-mm borosilicate glass capillaries (Warner Instrument, Hamden, CT) with a Narashige PC-10 needle puller so that the tip diameter was ~1 μm.

Needles were front-loaded with equal volumes of injectate solution using the ×40 objective. Inositol polyphosphates were suspended in deionized H_2O at a concentration of 100 μM for loading the needles. Equal volumes of solutions were injected into all cells. Live images of the cells were collected using the CCD camera. The growth rate was tracked over time by measuring the boundary position of the apex using the calibrated length measurement function of Lucia Image Analysis version 3.5 (Laboratory Imaging).

For the determination of pollen tube growth rates after the extracellular addition of Ins(3,4,5,6)P_4, Ins(1,3,4,5)P_4, Ins(1,3,4,5,6)P_5, and H_2O, pollen was cultured as described for the measurement of physical features of the apical regions. Growth rates were measured as described above, except that each rate was measured during a 1.5-min interval and 20 tubes were analyzed within 45 min after the start of treatment. Experiments were repeated twice, and the reported values were typical for both experiments.

Four considerations led to the design of experiments to test the effect of Ins(3,4,5,6)P_4 on Cl^- efflux. (1) Extracellular addition of Ins(3,4,5,6)P_4 was almost as effective as microinjection at inhibiting pollen tube growth. (2) Extracellular addition of Ins(3,4,5,6)P_4 rapidly induced an increase in apical cell volume that was close to the mean maximum volume limit established with the Cl^- channel blocker DIDS. (3) The affect of Ins(3,4,5,6)P_4 was specific: neither Ins(1,3,4,5)P_4 nor Ins(1,3,4,5,6)P_5 significantly affected growth rate or cell volume. The studies using Cl^- blockers indicated that perturbation of Cl^- flux correlated closely with the perturbation of both growth rate and cell volume. (4) The Cl^- efflux signal was dissipated rapidly, and oscillations were abolished by mechanical perturbation of the pollen tubes. Because of these considerations, experiments to test the effect of Ins(3,4,5,6)P_4 on Cl^- efflux were performed with extracellular addition of Ins(3,4,5,6)P_4.

Correlation of Growth Rate Oscillations with Chloride Efflux Oscillations and Cytological Dynamics

For correlation of pollen tube growth rate and Cl^- efflux (Figure 6), a 60×1.4 PlanApo or 100×1.3 PlanFluo oil-immersion objective was used under DIC optics, and sequential time-stamped images were captured using MetaMorph version 4.55 (Universal Imaging, West Chester, PA) and a Micromax 5-MHz cooled CCD camera (Princeton Instruments, Trenton, NJ) simultaneously with recording of Cl^- flux. The Cl^- oscillation values were converted from microvolt differential recordings (negative values) to absolute flux (positive values) to plot correlations. The time-stamped images were processed using a subpixel resolution pattern identification function to mark the boundary of the apex in each image (Track Object routine in MetaMorph). The boundary of the tube apex was defined further using a journal consecutively applying Fourier transformation (homomorphic 40%) and edge detection. The images were stacked, and the coordinates of each point were expressed as a velocity function of the point position. Data were collected into a set and exported to Microsoft Excel 4.0 for further analysis. When appropriate, a time-shift-corrected floating average was used (sampling 3 to 5 or <13 data points). The growth rate oscillations then were plotted with the Cl^- efflux oscillations chart using their common data points on the *x* axis (time).

For correlation of Cl^- efflux oscillations with growth and cytological dynamics (Figure 7), a 60×1.4 PlanApo or 100×1.3 PlanFluo oil-immersion objective was used under DIC optics, and images were captured at 1-s intervals using MetaMorph version 4.55 (Universal Imaging) and a Micromax 5-MHz cooled CCD camera (Princeton Instruments). Kinematic analysis was used to generate a kymogram from a 30-pixel-width transect. The transects were aligned on a new kymogram by normalizing the position of the cell wall boundary using a custom-made journal to allow a side-by-side comparison of the same relative area of the tube at sequential time points.

For correlation of cytological dynamics with growth (Figure 8), images were captured under data stream conditions at a rate of 0.21 s·image^{-1} using Lucia G Image Analysis version 4.5 (Laboratory Imaging), a Sony Power HAD 3CCD color video camera (Tokyo, Japan), and a 60×1.2 U-PlanApo water-immersion objective with DIC optics. Growth was measured at 5-s intervals by tracking the tip boundary using the edge-detection function of Lucia and measuring from a set reference point. Growth rates were calculated as moving averages after sampling of three data points.

Upon request, all novel materials described in this article will be made available in a timely manner for noncommercial research purposes. No restrictions or conditions will be placed on the use of any materials described in this article that would limit their use for noncommercial research purposes.

ACKNOWLEDGMENTS

We thank the editors and reviewers whose insightful comments led to the formulation of a much strengthened manuscript, and Richard Parton for critical reading of the first version of the manuscript. We also thank Jan Petrasek and Zdenek Opatrny for generous help with the time-lapse DIC imaging of pollen tube growth, and Neil Gliksman for developing the kymogram-aligning journal. L.Z. was supported by grants from the Czech Republic (Grant Agency Fund GA 521/99/1354 and Research Center "Signaling in Plants" [LN00A081MSMT]) and by a joint Czech-Portuguese Research Travel Grant. J.A.F. was supported by Fundação para a Ciência e Tecnologia (PRAXIS/C/BIA/11034/1998). The vibrating probe was financed partially by a grant from the Fundação Luso-Americana para o Desenvolvimento to J.A.F.

Received April 14, 2002; accepted June 18, 2002.

REFERENCES

Allen, G.J., Chu, S.P., Harrington, C.L., Schumacher, K., Hoffman, T., Tang, Y.Y., Grill, E., and Schroeder, J.I. (2001). A defined

range of guard cell calcium oscillation parameters encodes stomatal movements. Nature **411,** 1053–1057.

Allen, G.J., Chu, S.P., Schumacher, K., Shimazaki, C.T., Vafeados, D., Kemper, A., Hawke, S.D., Tallman, G., Tsien, R.Y., Harper, J.F., Chory, J., and Schroeder, J.I. (2000). Alteration of stimulus-specific guard cell calcium oscillations and stomatal closing in *Arabidopsis* det3 mutant. Science **289,** 2338–2342.

Amodeo, G., Srivastava, A., and Zeiger, E. (1992). Vanadate inhibits blue-light-stimulated swelling of *Vicia* guard cell protoplasts. Plant Physiol. **100,** 1567–1570.

Assmann, S.M. (1993). Signal transduction in guard cells. Annu. Rev. Cell Biol. **9,** 345–375.

Assmann, S.M., Simoncini, L., and Schroeder, J.I. (1985). Blue light activates electrogenic ion pumping in guard cell protoplasts of *Vicia faba*. Nature **318,** 285–287.

Astrom, H., Sorri, O., and Raudaskoski, M. (1995). Role of microtubules in the movement of the vegetative nucleus and generative cell in tobacco pollen tubes. Sex. Plant Reprod. **8,** 61–69.

Balla, T., Baukal, A.J., Hunyady, L., and Catt, K.J. (1989). Agonist-induced regulation of inositol tetrakisphosphate isomers and inositol pentakisphosphate in adrenal glomerulosa cells. J. Biol. Chem. **264,** 13605–13611.

Barbier-Brygoo, H., Vinauger, M., Colcombet, J., Ephritikhine, G., Frachisse, J., and Maurel, C. (2000). Anion channels in higher plants: Functional characterization, molecular structure and physiological role. Biochim. Biophys. Acta **1465,** 199–218.

Barrett, K.E., Smitham, J., Traynor-Kaplan, A., and Uribe, J.M. (1998). Inhibition of Ca^{2+}-dependent Cl^- secretion in T84 cells: Membrane target(s) of inhibition is agonist specific. Am. J. Physiol. Cell Physiol. **43,** C958–C965.

Bony, C., Roche, S., Shuichi, U., Sasaki, T., Crackower, M.A., Penninger, J., Mano, H., and Pucéat, M. (2001). A specific role of phosphatidylinositol 3-kinase γ: A regulation of autonomic Ca^{2+} oscillations in cardiac cells. J. Cell Biol. **152,** 717–727.

Brearley, C.A., and Hanke, D.E. (1996). Inositol phosphates in the duckweed *Spirodela polyrhiza* L. Biochem. J. **314,** 215–225.

Brearley, C.A., and Hanke, D.E. (2000). Metabolic relations of inositol 3,4,5,6-tetrakisphosphate revealed by cell permeabilization: Identification of inositol 3,4,5,6-tetrakisphosphate 1-kinase and inositol 3,4,5,6-tetrakisphosphate phosphatase activities in mesophyll cells. Plant Physiol. **122,** 1209–1216.

Caffrey, J.J., Safrany, S.T., Yang, Z., Yoshida, M., and Shears, S.B. (1999). The structural and functional diversity of inositol phosphates. In Phosphoinositides: Chemistry, Biochemistry and Biomedical Applications, Symposium Series 718, K.S. Bruzik, ed (Washington, DC: American Chemical Society), pp. 2–23.

Cai, G., Moscatelli, A., and Cresti, M. (1997). Cytoskeletal organization and pollen tube growth. Trends Plant Sci. **2,** 86–91.

Carew, M.A., Yang, X.N., Schultz, C., and Shears, S.B. (2000). myo-Inositol 3,4,5,6-tetrakisphosphate inhibits an apical calcium-activated chloride conductance in polarized monolayers of a cystic fibrosis cell line. J. Biol. Chem. **275,** 26906–26913.

Chen, Y., Simask, S.M., Niggel, J., Sigurdson, W.J., and Sachs, F. (1996). Ca^{2+} uptake in GH3 cells during hypotonic swelling: The sensory role of stretch-activated ion channels. Am. J. Physiol. **270,** C1790–C1798.

Cosgrove, D.J., and Hedrich, R. (1991). Stretch-activated chloride, potassium, and calcium channels coexisting in plasma membranes of guard cells of *Vicia faba* L. Planta **186,** 143–153.

Derksen, J., Pierson, E.S., and Traas, J.A. (1985). Microtubules in vegetative and generative cells of pollen tubes. Eur. J. Cell Biol. **38,** 42–48.

Derksen, J., Rutten, T., Van Amstel, T., de Win, A., Doris, F., and Steer, M. (1995). Regulation of pollen tube growth. Acta Bot. Neerl. **44,** 93–119.

Drøbak, B.K., Dewey, R.E., and Boss, W.F. (1999). Phosphoinositide kinases and the synthesis of polyphosphoinositides in higher plant cells. Int. Rev. Cytol. **189,** 95–130.

Feijó, J.A. (1999). The pollen tube oscillator: Towards a molecular mechanism of tip growth? In Fertilization in Higher Plants: Molecular and Cytological Aspects, M. Cresti, G. Cai, and A. Moscatelli, eds (Berlin: Springer), pp. 317–336.

Feijó, J.A., Sainhas, J., Hackett, G.R., Kunkel, J.G., and Hepler, P.K. (1999). Growing pollen tubes possess a constitutive alkaline band in the clear zone and a growth-dependent acidic tip. J. Cell Biol. **144,** 483–496.

Feijó, J.A., Sainhas, J., Holdaway-Clarke, T., Cordeiro, S., Kunkel, J.G., and Hepler, P.K. (2001). Cellular oscillations and the regulation of growth: The pollen tube paradigm. Bioessays **23,** 86–94.

Franklin-Tong, V.E., Drøbak, B.K., Allan, A.C., and Trewavas, A.J. (1996). Growth of pollen tubes of *Papaver rhoeas* is regulated by a slow-moving calcium wave propagated by inositol 1,4,5-trisphosphate. Plant Cell **8,** 1305–1321.

Franklin-Tong, V.E., Hackett, G., and Hepler, P.K. (1997). Ratio-imaging of Ca^{2+} in the self-incompatibility response in pollen tubes of *Papaver rhoeas*. Plant J. **12,** 1375–1386.

Fu, Y., Wu, G., and Yang, Z. (2001). Rop GTPase-dependent dynamics of tip-localized F-actin controls tip growth in pollen tubes. J. Cell Biol. **152,** 1019–1032.

Geitmann, A., and Cresti, M. (1998). Ca^{2+} channels control the rapid extensions in pulsatory growth of *Petunia hybrida* pollen tubes. J. Plant Physiol. **152,** 439–447.

Geitmann, A., Li, Y.Q., and Cresti, M. (1996). The role of the cytoskeleton and dictyosome activity in the pulsatory growth of *Nicotiana tabacum* and *Petunia hybrida* pollen tubes. Bot. Acta **109,** 102–109.

Goddard, H., Manison, N.F.H., Tomos, D., and Brownlee, C. (2000). Elemental propagation of calcium signals in response-specific patterns determined by environmental stimulus strength. Proc. Natl. Acad. Sci. USA **97,** 1932–1937.

Hedrich, R., Busch, H., and Raschke, K. (1990). Ca^{2+} and nucleotide dependent regulation of voltage dependent anion channels in the plasma membrane of guard cells. EMBO J. **9,** 3889–3892.

Hepler, P.K., Vidali, L., and Cheung, A.Y. (2001). Polarized cell growth in higher plants. Annu. Rev. Cell Dev. Biol. **17,** 159–187.

Ho, M.W., Kaetzel, M.A., Armstrong, D.L., and Shears, S.B. (2001). Regulation of a human chloride channel, a paradigm for integrating input from calcium, type II calmodulin-dependent protein kinase, and inositol 3,4,5,6-tetrakisphosphate. J. Biol. Chem. **276,** 18673–18680.

Ho, M.W.Y., Carew, M.A., Yang, X., and Shears, S.B. (2000). Regulation of chloride channel conductance by $Ins(3,4,5,6)P_4$, a phosphoinositide-initiated signalling pathway that acts downstream of $Ins(1,4,5)P_3$. In Biology of Phosphoinositides, S. Cockcroft, ed (Oxford, UK: Oxford University Press), pp. 298–319.

Holdaway-Clarke, T., Feijó, J.A., Hackett, G.R., Kunkel, J.G., and Hepler, P.K. (1997). Pollen tube growth and the intracellular cytosolic calcium gradient oscillate in phase while extracellular calcium influx is delayed. Plant Cell **9,** 1999–2010.

Irvine, R.F., and Schell, M.J. (2001). Back in the water: The return of the inositol phosphates. Nat. Rev. **2,** 327–338.

Ismailov, I.I., Fuller, C.M., Berdiev, B.K., Shlyonsky, V.G., Benos, D.J., and Barrett, K.E. (1996). A biologic function for an "orphan" messenger: D-*myo*-inositol 3,4,5,6-tetrakisphosphate selectively blocks epithelial calcium-activated chloride channels. Proc. Natl. Acad. Sci. USA **93,** 10505–10509.

Joos, U., van Aken, J., and Kristen, U. (1994). Microtubules are involved in maintaining the cellular polarity in pollen tubes of *Nicotiana silvestris*. Protoplasma **179,** 5–15.

Kochian, L.V., Shaff, J.E., Kühtreiber, W.M., Jaffe, L.F., and Lucas, W.J. (1992). Use of an extracellular, ion-selective, vibrating microelectrode system for the quantification of K^+, H^+, and Ca^{2+} fluxes in maize roots and maize suspension cells. Planta **188,** 601–610.

Kost, B., Lemichez, E., Spielhofer, P., Hong, Y., Tolias, K., Carpenter, C., and Chua, N.-H. (1999). Rac homologues and compartmentalized phosphatidylinositol 4,5-bisphosphate act in a common pathway to regulate polar pollen tube growth. J. Cell Biol. **145,** 317–330.

Kost, B., Spielhofer, P., and Chua, N.-H. (1998). A GFP-mouse talin fusion protein labels plant actin filaments *in vivo* and visualizes the actin cytoskeleton in growing pollen tubes. Plant J. **16,** 393–401.

Kropman, M.F., and Bakker, H.J. (2001). Dynamics of water molecules in aqueous solvation shells. Science **291,** 2118–2120.

Kühtreiber, W.M., and Jaffe, L.F. (1990). Detection of extracellular calcium gradients with a calcium-specific vibrating electrode. J. Cell Biol. **110,** 1565–1573.

Lancelle, S.A., and Hepler, P.K. (1991). Association of actin with cortical microtubules revealed by immunogold localization in *Nicotiana* pollen tubes. Protoplasma **165,** 167–172.

Lemtiri-Chlieh, F., MacRobbie, E.A.C., and Brearley, C.A. (2000). Inositol hexakisphosphate is a physiological signal regulating the K^+-inward rectifying conductance in guard cells. Proc. Natl. Acad. Sci. USA **97,** 8687–8692.

Liu, K., and Luan, S. (1998). Voltage-dependent K^+ channels as targets of osmosensing in guard cells. Plant Cell **10,** 1957–1970.

Malhó, R. (1998). Role of 1,4,5-inositol trisphosphate-induced Ca^{2+} release in pollen tube orientation. Sex. Plant Reprod. **11,** 231–235.

Malhó, R., Read, N.D., Trewavas, A.J., and Pais, M.S. (1994). Role of cytosolic free calcium in the reorientation of pollen tube growth. Plant J. **5,** 331–341.

Marten, I., Lohse, G., and Hedrich, R. (1991). Plant growth hormones control voltage-dependent activity of anion channels in plasma membrane of guard cells. Nature **353,** 758–762.

Mascarenhas, J.P., and LaFountain, J. (1972). Protoplasmic streaming, cytochalasin B, and growth of the pollen tube. Tissue Cell **4,** 11–14.

Meijer, H.J.G., Divecha, N., van den Ende, H., Musgrave, A., and Munnik, T. (1999). Hyperosmotic stress induces rapid synthesis of phosphatidyl-D-inositol 3,5-bisphosphate in plant cells. Planta **208,** 294–298.

Mennitti, F.S., Oliver, K.G., Putney, J.W., Jr., and Shears, S.B. (1993). Inositol phosphates and cell signalling: New view of $InsP_5$ and $InsP_6$. Trends Biochem. Sci. **18,** 53–56.

Messerli, M.A., Créton, R., Jaffe, L.F., and Robinson, K.R. (2000). Periodic increases in elongation rate precede increases in cytosolic Ca^{2+} during pollen tube growth. Dev. Biol. **222,** 84–98.

Messerli, M.A., Danuser, G., and Robinson, K.R. (1999). Pulsatile influxes of H^+, K^+, and Ca^{2+} lag growth pulses of *Lilium longiflorum*. J. Cell Sci. **112,** 1497–1509.

Messerli, M.A., and Robinson, K.R. (1997). Tip localized Ca^{2+} pulses are coincident with peak pulsatile growth rates in pollen tubes of *Lilium longiflorum*. J. Cell Sci. **110,** 1269–1278.

Messerli, M.A., and Robinson, K.R. (1998). Cytoplasmic acidification and current influx follow growth pulses of *Lilium longiflorum* pollen tubes. Plant J. **16,** 87–91.

Miller, D.D., Callaham, D.A., Gross, D.J., and Hepler, P.K. (1992). Free Ca^{2+} gradient in growing pollen tubes of *Lilium*. J. Cell Sci. **101,** 7–12.

Miller, D.D., Lancelle, S.A., and Hepler, P.K. (1996). Actin microfilaments do not form a dense meshwork in *Lilium longiflorum* pollen tube tips. Protoplasma **195,** 123–132.

Miller, D.D., Scordilis, S.P., and Hepler, P.K. (1995). Identification and localization of three classes of myosins in pollen tubes of *Lilium longiflorum* and *Nicotiana alata*. J. Cell Sci. **108,** 2549–2553.

Munnik, T., Irvine, R.F., and Musgrave, A. (1998). Phospholipid signalling in plants. Biochim. Biophys. Acta **1389,** 222–272.

Munnik, T., and Meijer, H.J.G. (2001). Osmotic stress activates distinct lipid and MAPK signaling pathways in plants. FEBS Lett. **498,** 172–178.

Nilius, B., Prenen, J., Voets, T., Eggermont, J., Bruzik, K.S., Shears, S.B., and Droogmans, G. (1998). Inhibition by inositoltetrakisphosphates of calcium- and volume-activated Cl^- currents in macrovascular endothelial cells. Pfluegers Arch. **435,** 637–644.

Pical, C., Westergren, T., Dove, S.K., Larsson, C., and Sommarin, M. (1999). Salinity and hyperosmotic stress induce rapid increases in phosphatidylinositol 4,5-bisphosphate, diacylglycerol pyrophosphate, and phosphatidylcholine in *Arabidopsis thaliana* cells. J. Biol. Chem. **274,** 38232–38240.

Pierson, E.S., and Cresti, M. (1992). Cytoskeleton and cytoplasmic organization of pollen tubes. Int. Rev. Cytol. **140,** 73–125.

Pierson, E.S., Li, Y.Q., Zhang, H.Q., Willemse, M.T.M., Linskens, H.F., and Cresti, M. (1995). Pulsatory growth of pollen tubes: Investigation of a possible relationship with the periodic distribution of cell wall components. Acta Bot. Neerl. **44,** 121–128.

Pierson, E.S., Miller, D.D., Callaham, D.A., Shipley, A.M., Rivers, B.A., Cresti, M., and Hepler, P.K. (1994). Pollen tube growth is coupled to the extracellular calcium ion and the intracellular calcium gradient: Effect of BAPTA-type buffers and hypertonic media. Plant Cell **6,** 1815–1828.

Pierson, E.S., Miller, D.D., Callaham, D.A., Van Aken, J., Hackett, G., and Hepler, P.K. (1996). Tip-localized calcium entry fluctuates during pollen tube growth. Dev. Biol. **174,** 160–173.

Pittet, D., Lew, D.P., Mayr, G.W., Monod, A., and Schlegel, W. (1989). Chemoattractant receptor promotion of Ca^{2+} influx across the plasma membrane of HL-60 cells: A role for cytosolic free calcium elevations and inositol 1,3,4,5-tetrakisphosphate production. J. Biol. Chem. **264,** 7251–7261.

Rathore, K.S., Cork, J., and Robinson, K.R. (1991). A cytoplasmic gradient of Ca^{2+} is correlated with the growth of lily pollen tubes. Dev. Biol. **148,** 612–619.

Rudolf, M.T., Li, W.H., Wolfson, N., Traynor-Kaplan, A.E., and Schultz, C. (1998). 2-Deoxy derivative is a partial agonist of the intracellular messenger inositol 3,4,5,6-tetrakisphosphate in the epithelial cell line T-84. J. Med. Chem. **41,** 3635–3644.

Sanders, D., and Bethke, P. (2000). Membrane transport. In Biochemistry and Molecular Biology of Plants, B.B. Buchanan, W. Gruissem, and R.L. Jones, eds (Rockville, MD: American Society of Plant Physiologists), pp. 110–158.

Satter, R.L., Morse, M.J., Lee, Y., Crain, R.C., Coté, G.G., and Moran, N. (1988). Light- and clock-controlled leaflet movements in *Samanea saman*: A physiological, biophysical and biochemical analysis. Bot. Acta **101,** 205–213.

Schroeder, J.I. (1995). Anion channels as central mechanisms for signal transduction in guard cells and putative functions in roots for plant-soil interactions. Plant Mol. Biol. **28,** 353–361.

Schroeder, J.I., Allen, G.J., Hugouvieux, V., Kwak, J.M., and Warner, D. (2001). Guard cell signal transduction. Annu. Rev. Plant Physiol. Plant Mol. Biol. **52,** 627–658.

Schroeder, J.I., and Hedrich, R. (1989). Involvement of ion channels and active transport in osmoregulation and signaling of higher plant cells. Trends Biochem. Sci. **14,** 187–192.

Shabala, S., Babourina, O., and Newman, I. (2000). Ion-specific mechanisms of osmoregulation in bean mesophyll cells. J. Exp. Bot. **51,** 1243–1253.

Shears, S.B. (1996). Inositol pentakis- and hexakisphosphate metabolism adds versatility to the actions of inositol polyphosphates: Novel effects on ion channels and protein traffic. In *myo*-Inositol Phosphates, Phosphoinositides, and Signal Transduction: Subcellular Biochemistry, Vol. 26, B.B. Biswas and S. Biswas, eds (New York: Plenum Press), pp 187–226.

Shipley, A.M., and Feijó, J.A. (1999). The use of the vibrating probe technique to study steady extracellular currents during pollen germination and tube growth. In Fertilization in Higher Plants: Molecular and Cytological Aspects, M. Cresti, G. Cai, and A. Moscatelli, eds (Berlin: Springer), pp. 235–252.

Stephens, L.R., Hawkins, P.T., Barker, C.J., and Downes, P.C. (1988). Synthesis of myo-inositol 1,3,4,5,6-pentakisphosphate from inositol phosphates generated by receptor activation. Biochem. J. **253,** 721–733.

Stevenson, J.M., Perera, I., Heilmann, I., Persson, S., and Boss, W.F. (2000). Inositol signaling and plant growth. Trends Plant Sci. **5,** 252–258.

Takahashi, K., Isobe, M., Knight, M.R., Trewavas, A.J., and Muto, S. (1997). Hypoosmotic shock induces increases in cytosolic Ca^{2+} in tobacco suspension culture cells. Plant Physiol. **113,** 587–594.

Tang, X.W., Liu, G.Q., Yang, Y., Zheng, W.L., Wu, B.C., and Nie, D.T. (1992). Quantitative measurement of pollen tube growth and particle movement. Acta Bot. Sinica **34,** 893–898.

Taylor, A., Manison, N., and Brownlee, C. (1997). Regulation of channel activity underlying cell volume and polarity signals in *Fucus*. J. Exp. Bot. **48,** 579–588.

Taylor, L.P., and Hepler, P.K. (1997). Pollen germination and tube growth. Annu. Rev. Plant Physiol. Plant Mol. Biol. **48,** 461–491.

Teodoro, A.E., Zingarelli, L., and Lado, P. (1998). Early changes in Cl^- efflux and H^+ extrusion induced by osmotic stress in *Arabidopsis thaliana* cells. Physiol. Plant. **102,** 29–37.

Vajanaphanich, M., Schultz, C., Rudolf, M.T., Wasserman, M., Enyedi, P., Craxton, A., Shears, S.B., Tsien, R.Y., Barrett, K.E., and Traynor-Kaplan, A. (1994). Long-term uncoupling of chloride secretion from intracellular calcium levels by Ins(3,4,5,6)P_4. Nature **371,** 711–714.

Ward, J.M., Pei, Z.-M., and Schroeder, J.I. (1995). Roles of ion channels in initiation of signal transduction in higher plants. Plant Cell **7,** 833–844.

Xie, W., Kaetzel, M.A., Bruzik, K.S., Dedman, J.R., Shears, S.B., and Nelson, D.J. (1996). Inositol 3,4,5,6-tetrakisphosphate inhibits the calmodulin-dependent protein kinase II-activated chloride conductance in T84 colonic epithelial cells. J. Biol. Chem. **271,** 14092–14097.

Xie, W., Solomons, K.R.H., Freeman, S., Kaetzel, M.A., Bruzik, K.S., Nelson, D.J., and Shears, S.B. (1998). Regulation of Ca^{2+}-dependent Cl^- conductance in a human colonic epithelial cell line (T84): Cross-talk between Ins(3,4,5,6)P_4 and protein phosphatases. J. Physiol. **510**, 661–673.

Yang, X.N., Rudolf, M., Carew, R.A., Yoshida, M., Nerreter, V., Riley, A.M., Chung, S.K., Bruzik, K.S., Potter, B.V.L., Schultz, C., and Shears, S.B. (1999). Inositol 1,3,4-trisphosphate acts in vivo as a specific regulator of cellular signaling by inositol 3,4,5,6-tetrakisphosphate. J. Biol. Chem. **274,** 18973–18980.

Yokuta, E., Muto, S., and Shimmen, T. (1999). Inhibitory regulation of higher plant myosin by Ca^{2+} ions. Plant Physiol. **119,** 231–239.

Zonia, L., Cordeiro, S., and Feijó, J.A. (2001). Ion dynamics and the control of hydrodynamics in the regulation of pollen tube growth. Sex. Plant Reprod. **14,** 111–116.